Annu. Rev. Earth Planet. Sci. 1994. 22:207–37

MECHANICS OF EARTHQUAKES

H. Kanamori

Seismological Laboratory, California Institute of Technology, Pasadena, California 91125

KEY WORDS: stress drop, static stress drop, dynamic stress drop, kinetic friction

INTRODUCTION

An earthquake is a sudden rupture process in the Earth's crust or mantle caused by tectonic stress. To understand the physics of earthquakes it is important to determine the state of stress before, during, and after an earthquake. There have been significant advances in seismology during the past few decades, and some details on the state of stress near earthquake fault zones are becoming clearer. However, the state of stress is generally inferred indirectly from seismic waves which have propagated through complex structures. The stress parameters thus determined depend on the specific seismological data, methods, and assumptions used in the analysis, and must be interpreted carefully.

This paper reviews recent seismological data pertinent to this subject, and presents simple mechanical models for shallow earthquakes. Scholz (1989), Brune (1991), Gibowicz (1986), and Udias (1991) recently reviewed this subject from a different perspective, and we will try to avoid duplication with these papers as much as possible. Because of the limited space available, this review is not intended to be an exhaustive summary of the literature, but reflects the author's own view on the subject.

Throughout this paper we use the following notation unless indicated otherwise: α = P-wave velocity, β = S-wave velocity, V_r = rupture velocity, $\dot{U}$ = fault particle-motion velocity, σ_0 = tectonic shear stress on the fault plane before an earthquake, σ_1 = tectonic shear stress on the fault plane after an earthquake, $\Delta\sigma = \sigma_0 - \sigma_1$ = static stress drop, σ_f = kinetic frictional stress during faulting, $\Delta\sigma_d = \sigma_0 - \sigma_f$ = dynamic (kinetic) stress drop, S = fault area, D = fault offset, $\dot{D} = 2\dot{U}$ = fault offset particle vel-

0084–6597/94/0515–0207$05.00

ocity, M = earthquake magnitude, μ = rigidity, $M_0 = \mu DS$ = seismic moment.

TECTONIC STRESS

The rupture zones of earthquakes are usually planar (fault plane), but occasionally exhibit a complex geometry. The stress distribution near a fault zone varies as a function of time and space in a complex manner. Before and after an earthquake (interseismic period), the stress varies gradually over a time scale of decades and centuries, and during an earthquake (coseismic period) it varies on a time scale of a few seconds to a few minutes.

The stress variation during an interseismic period can be considered quasi-static. It varies spatially with stress concentration near locations with complex fault geometry. We often simplify the situation by considering static stress averaged over a scale length of kilometers. We call this stress field the "macroscopic static stress field." In contrast, we call the stress field with a scale length of local fault complexity the "microscopic static stress field."

During an earthquake, stress changes very rapidly. It decreases in most places on the fault plane, but it may increase at some places, especially near the edge of a fault where stress concentration occurs. We call the stress field averaged over a time scale of faulting the "macroscopic dynamic stress field," and that with a time scale of rupture initiation, the "microscopic dynamic stress field."

Macroscopic Static Stress Field

Figure 1 shows a schematic time history of macroscopic static stress over three earthquake cycles. After an earthquake the shear stress on the fault

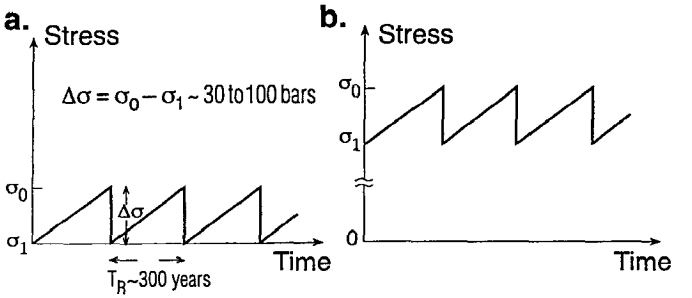

Figure 1 Schematic figure showing temporal variations of macroscopic (quasi-)static stress on a fault plane. (*a*) Weak fault model. (*b*) Strong fault model.

monotonically increases from σ_1 to σ_0 during an interseismic period. When it approaches σ_0, the fault fails causing an earthquake, and the stress drops to σ_1, and a new cycle begins. The stress difference $\Delta\sigma = \sigma_0 - \sigma_1$ is the static stress drop, and T_R is the repeat time. For a typical sequence along active plate boundaries, $\Delta\sigma \approx 30$ to 100 bars, and $T_R \approx 300$ years. (The numerical values given in the text are representative values for illustration purposes only; more details will be given in the section for each parameter.)

The absolute value of σ_0 and σ_1 cannot be determined directly with seismological methods; only the difference, $\Delta\sigma = \sigma_0 - \sigma_1$, can be determined. If fault motion occurs against kinetic (dynamic) friction, σ_f, repeated occurrence of earthquakes should result in a local heat flow anomaly along the fault zone. From the lack of a local heat flow anomaly along the San Andreas fault, a relatively low value, 200 bars or less, has been suggested for σ_f (Brune et al 1969; Henyey & Wasserburg 1971; Lachenbruch & Sass 1973, 1980). More recent studies on the stress on the San Andreas fault zone also suggest a low stress—less than a few hundred bars (Mount & Suppe 1987, Zoback et al 1987). However, the strength of rocks (frictional strength) measured in the laboratory suggests that shear stress on faults is high, probably higher than 1 kbar (Byerlee 1970, Brace & Byerlee 1966). Figures 1*a* and 1*b* show the two end-member models, the weak fault model ($\sigma_0 \approx 200$ bars), and the strong fault model ($\sigma_0 \approx 2$ kbars). In these simple models "strength of fault" refers to σ_0. Actually, σ_0 and σ_1 may vary significantly from place to place and from event to event; the loading rate may also change as a function of time so that the time history is not expected to be as regular as indicated in Figure 1.

Microscopic Static Stress Field

An earthquake fault is often modeled with a crack in an elastic medium. Figure 2 shows the distribution of shear stress near a crack tip (e.g. Knopoff

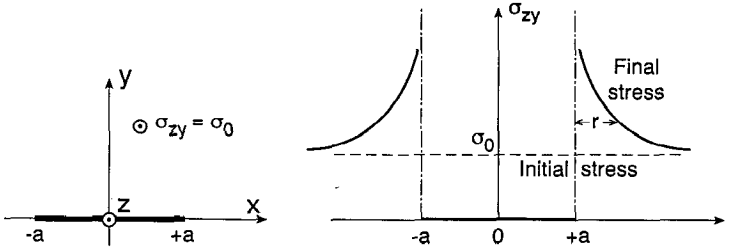

Figure 2 Static stress field near a crack tip. (*Left*) Geometry. A 2-dimensional crack with a width of $2a$ extending from $z = -\infty$ to $+\infty$ is formed under shear stress $\sigma_{zy} = \sigma_0$. (*Right*) Shear stress σ_{zy} before (*dashed line*) and after (*solid curves*) crack formation.

1958). For an infinitely thin crack in a purely elastic medium, the stress (σ_{zy} in Figure 2) is unbounded at the crack tip, and decreases as $1/\sqrt{r}$ as the distance r from the crack tip increases (i.e. inverse square-root singularity). In a real medium, the material near the crack tip yields at a certain stress level (yield stress) causing the stress near the crack tip to be finite. Nevertheless, the behavior shown in Figure 2 is considered to be a good qualitative representation of static stress field near a fault tip.

In actual fault zones, the strength is probably highly nonuniform, and many local weak zones ("micro-faults") and geometrical irregularities are distributed as shown in Figure 3. As the fault system is loaded by tectonic stress σ, stress concentration occurs at the tip of many micro-faults as shown in Figure 3. Near the areas of stress concentration, the stress can be much higher than the loading stress σ. As the stress near the fault tip reaches a threshold value determined by some rupture criteria (e.g. Griffith 1920), and if the friction characteristic is favorable for unstable sliding (e.g. Dieterich 1979, Rice 1983, Scholz 1989), the fault ruptures. As mentioned earlier, the strength of the fault refers to the tectonic stress σ at the time of rupture initiation ($=\sigma_0$), but not to the stress near the fault tip where the stress is much higher than σ_0.

The microscopic stress distribution is mainly controlled by the distribution of micro-faults and is very complex, but the average over a scale length of kilometers is probably close to the loading stress.

Macroscopic Dynamic Stress Field

Although the dynamic stress change during faulting can be very complex, its macroscopic behavior can be described as follows (Brune 1970). If, at $t = 0$, the fault ruptures instantaneously under tectonic stress σ_0, then the displacement of a point just next to the fault will be as shown in Figure

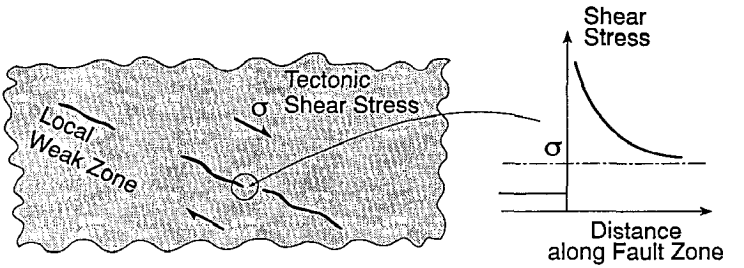

Figure 3 Schematic figure showing a fault zone in the Earth's crust. Heavy solid curves indicate local weak zones (micro-faults) under tectonic shear stress σ. The figure on the right shows stress concentration near the tip of micro-faults. The shear stress on the micro-fault is not necessarily 0, but is significantly smaller than the loading stress σ.

4*a*. Fault motion is resisted by kinetic friction σ_f during slippage so that the difference $\Delta\sigma_d = \sigma_0 - \sigma_f$ is the effective stress that drives fault motion, and is called the dynamic stress drop. In general $\Delta\sigma_d$ varies with time. Following Brune (1970), $\Delta\sigma_d$ can be related to the particle velocity $\dot{U}$ of one side of the fault. After rupture initiation, the shear disturbance propagates in the direction perpendicular to the fault (Figure 4*a*). At time t it reaches the distance βt, beyond which the disturbance has not arrived. Denoting the displacement on the fault at this time by $u(t)$, the instantaneous strain is $u(t)/\beta t$. Since this is caused by $\Delta\sigma_d$,

$$\Delta\sigma_d = \mu u(t)/\beta t$$

from which we obtain

$$u(t) = \Delta\sigma_d \beta t/\mu \quad \text{and} \quad \dot{u}(t) = (\Delta\sigma_d/\mu)\beta = \dot{U} = \text{constant}. \tag{1}$$

Curve (1) in Figure 4*b* shows $u(t)$ for this case.

As the fault rupture encounters some obstacle or the end of the fault, the fault motion slows down and eventually stops as shown by curve (2) in Figure 4*b*. This result is in good agreement with the numerical result by Burridge (1969).

Since the fault rupture is not instantaneous, but propagates with a finite rupture velocity V_r, which is usually about 70 to 80% of β, the actual macroscopic particle motion is slower than that given by (1). Also, the beginning of rupture can no longer be given by a linear function of time (e.g. Ida & Aki 1972). Nevertheless, the macroscopic behavior can be described by (1) with deceleration of about a factor of 2, as shown by

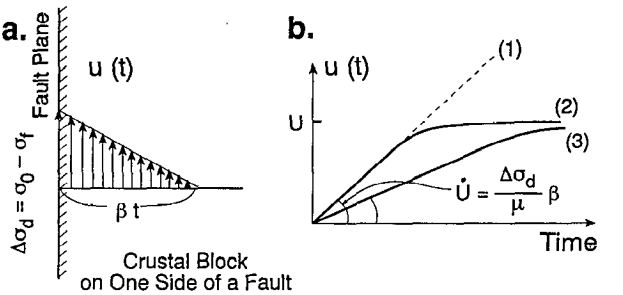

Figure 4 (*a*) Displacement at time t as a function of fault-normal distance from the fault. The stress on the fault is the effective stress (dynamic stress drop) $\Delta\sigma_d = \sigma_0 - \sigma_f$. The disturbance has propagated to a distance of βt. (*b*) Particle motion of one side of the fault as a function of time. Curve (1) is for an infinitely long fault when the $\Delta\sigma_d$ is applied instantaneously. Curve (2) is for a finite fault. Curve (3) is for a finite fault when $\Delta\sigma_d$ is applied as a propagating stress.

curve (3) in Figure 4*b*. Numerical results by Hanson et al (1971), Madariaga (1976), and Richards (1976) support this conclusion. If we denote the offset and duration of slip by D $(=2U)$ and T_r, then the average macroscopic particle velocity is $\langle \dot{U} \rangle = D/(2T_r)$. Thus, Equation (1) suggests

$$\langle \dot{U} \rangle = \frac{1}{c_1}\left(\frac{\Delta\sigma_d}{\mu}\right)\beta, \quad \text{and} \quad \Delta\sigma_d = c_1\left(\frac{\mu}{\beta}\right)\langle \dot{U} \rangle, \tag{2}$$

where c_1 is a constant which is of the order of 2.

Microscopic Dynamic Stress Field

Since the theory of cracks in an elastic medium is well established, it is most convenient to use the results from crack theory to understand the dynamic stress field during faulting. In a real fault zone, the fault geometry is complex, and the strength and material properties are heterogeneous so that the stress field is very different from that computed for a simple crack. Nevertheless, the results for a simple crack provide a useful insight regarding the general property of stress and particle motion during faulting. Many theoretical studies have been made on this subject (Kostrov 1966, Burridge 1969, Takeuchi & Kikuchi 1971, Kikuchi & Takeuchi 1971, Ida 1972, Richards 1976, Madariaga 1976). Here we briefly describe the results for steady-state crack propagation described by Freund (1979). The geometry of the crack is shown in Figure 5*a*. (This is called the antiplane shear mode III problem.) The crack expands in the $+x$ direction under uniform far-field stress $\sigma_{yz} = \sigma_0$. The crack propagates at a constant velocity $V_r < \beta$ (steady propagation). The crack surface extends from $-a$ to a over which the stress is equal to the kinetic friction σ_f. Then Equations (21) and (22) of Freund (1979) yield:

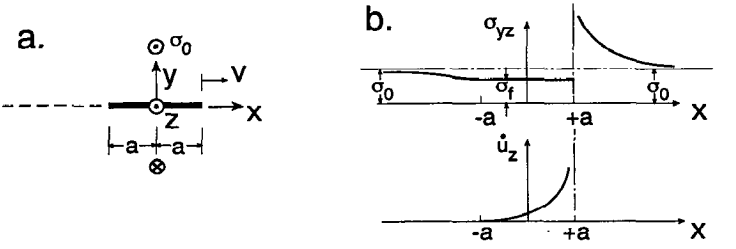

Figure 5 Steady crack propagation. (*a*) Geometry (same as Figure 2*a*). A crack propagating in the x direction at a velocity of V_r. (*b*) The shear stress σ_{zy} and particle velocity $\dot{u}_z$ as a function of distance.

$$\dot{u}_z = 0, \quad \sigma_{yz} = (\sigma_0 - \sigma_f)\left(\sqrt{\frac{x+a}{x-a}} - 1\right) + \sigma_0 \quad \text{for} \quad x > a$$

$$\dot{u}_z = \frac{V_r}{\mu}(\sigma_0 - \sigma_f)\sqrt{\frac{a+x}{a-x}}, \quad \sigma_{yz} = \sigma_f \quad \text{for} \quad -a < x < a$$

$$\dot{u}_z = 0, \quad \sigma_{yz} = (\sigma_0 - \sigma_f)\left(\sqrt{\frac{x+a}{x-a}} - 1\right) + \sigma_0 \quad \text{for} \quad x < -a. \tag{3}$$

From the condition that there be no stress singularity at the trailing edge at $x = -a$,

$$(\sigma_0 - \sigma_f) = \frac{\mu U}{2\pi a}\sqrt{1 - \left(\frac{V_r}{\beta}\right)^2}, \tag{4}$$

where U is the total displacement of one side of the crack. The stress difference $\sigma_0 - \sigma_f$ is the dynamic stress drop $\Delta\sigma_d$ defined earlier.

These results are graphically shown in Freund (1979) and are reproduced in Figure 5*b*. The typical inverse square-root singularity ($1/\sqrt{x-a}$) is seen for σ_{yz} ahead of the leading edge, and for $\dot{u}_z$ just behind it.

The degree of singularity depends on the physical condition near the crack tip, e.g. the dependence of the cohesive force on velocity and displacement. In a real fault zone, because of the finite strength of the material, the velocity and stress must be finite.

In principle, we should be able to determine the time history of particle velocity from seismological observations and compare it to Equation (3), but in practice it is difficult to determine this uniquely. Seismologically, one observes convolution of the local slip function shown in Figure 4*b* and the rupture propagation effect, and it is difficult to separate these two factors. Most commonly, seismologists can determine only the average particle velocity. Using (3) we obtain the average particle velocity

$$\langle \dot{U} \rangle = \frac{1}{2a}\int_{-a}^{+a} \dot{u}_z\, dx = \frac{\pi V_r}{2\mu}(\sigma_0 - \sigma_f),$$

from which

$$(\sigma_0 - \sigma_f) = \Delta\sigma_d = \frac{2\mu}{\pi V_r}\langle \dot{U} \rangle \approx \left(\frac{\mu}{\beta}\right)\langle \dot{U} \rangle, \tag{5}$$

where $V_r = 0.7\beta$ is assumed. Equation (5) agrees with Equation (2) except for the factor c_1, which is of the order of 2. Considering all the uncertainties in the determination of $\langle \dot{U} \rangle$ and the model, this much of uncertainty is

inevitable. For simplicity's sake we will use Equation (5) in the following discussion, but this uncertainty (a factor of 2) must be borne in mind in interpreting the particle velocity in terms of $\Delta\sigma_d$. Husseini (1977) obtained a similar expression.

The large particle velocity near the leading edge contributes to excitation of high-frequency accelerations, but the actual mechanism is complex. For example, Yamashita (1983) explained the observed accelerations in terms of abrupt changes in rupture propagation, but exactly how high-frequency accelerations are excited is still an unresolved problem. High-frequency accelerations can be excited by irregular rupture velocity, sudden changes in material strength or sudden changes in frictional characteristics (Aki 1979). Chen et al (1987) showed that heterogeneities of both stress drop and cohesion are the main factors that control the growth, cessation, and healing of the crack, and that the complexities in seismic radiation are caused by the complex healing process as well as complex rupture propagation.

In the discussion above, V_r is assumed constant. In a more realistic case of spontaneous crack propagation, however, V_r is determined by the property of the material (cohesive energy, surface energy) and the geometry of the crack, and the degree of stress concentration near the crack tip changes drastically (Kostrov 1966, Kikuchi & Takeuchi 1971, Burridge 1969, Richards 1976). However, in most seismological applications, $V_r/\beta \approx 0.7$ to 0.8 and the model of steady subsonic crack propagation is considered reasonable.

SEISMOLOGICAL OBSERVATIONS

Static Stress Drop

Static stress drop $\Delta\sigma$ can be determined by the ratio of displacement u to an appropriate scale length $\tilde{L}$ of the area over which the displacement occurred:

$$\Delta\sigma = c\mu(u/\tilde{L}). \tag{6}$$

This scale length could be the fault length L, the fault width W, or the square root of fault area S, depending on the fault geometry.

Since the stress and strength distributions near a fault are nonuniform, the slip and stress drop are in general a complex function of space. In most applications, we use the stress drop averaged over a certain area, e.g. the entire fault plane. Locally, the stress drop can be much higher than the average (Madariaga 1979). To be exact, the average stress drop is the spatial average of the stress drop. However, the limited resolution of seismological methods often allows determinations of only the average

displacement over the fault plane, which in turn is used to compute the average stress drop.

Stress drops have been estimated using the following methods:

1. From D and $\tilde{L}$ estimated from geodetic data.
2. From D estimated from surface break, and S estimated from the aftershock area.
3. From seismic moment M_0, and S estimated from either the aftershock area, surface break, or geodetic data.
4. From M_0, and $\tilde{L}$, estimated from the source pulse width τ, or the characteristic frequency (often called the corner frequency) f_0 of the source spectrum.
5. From the slip distribution on the fault plane determined from high-resolution seismic data.
6. From a combination of the above.

Method 1 was used by Tsuboi (1933) for the 1927 Tango, Japan, earthquake. Tsuboi concluded that the strain associated with the earthquake is of the order of 10^{-4} which translates to $\Delta\sigma$ of 30 bars ($\mu = 3 \times 10^{11}$ dyne/cm^2 is assumed). Chinnery (1964) also used this method to conclude that the stress drops of earthquakes are about 10 to 100 bars.

Method 2 is used when geodetic data are not available. Unfortunately the surface break does not necessarily represent the slip at depth (some earthquakes do not produce a surface break, e.g. the 1989 Loma Prieta, California, earthquake). In general, the overall extent of the aftershock area can be taken as the extent of the rupture zone. Although this interpretation is not correct in detail (for many earthquakes, the aftershocks do not occur in the area of large slip, but in the surrounding areas), the overall distribution of the aftershocks appears to coincide with the extent of the rupture zone. However, the aftershock area usually expands as a function of time, and there is always some ambiguity regarding identification of aftershocks and the aftershock area. Most frequently, the aftershock area defined at about one day after the main shock is used for this purpose (Mogi 1968), but this definition is somewhat arbitrary.

Method 3 is most commonly used for large earthquakes. The seismic moment M_0 can be reliably determined from long-period surface waves and body waves for most large earthquakes in the world using the data from seismic stations distributed worldwide. When the fault geometry is fixed, the seismic moment is a scalar quantity given by $M_0 = \mu DS$. From M_0 and S, D can be determined. If we define the scale length of the fault by $\tilde{L} = S^{1/2}$, the average strain change is $\varepsilon = c_1 D/S^{1/2}$ where c_1 is a constant determined by the geometry of the fault, and is usually of the order of 1. Then the stress drop is

$$\Delta\sigma = \mu\varepsilon = c_1\mu D/S^{1/2} \tag{7}$$

Method 4 is frequently used for relatively small ($M < 5$) earthquakes. For these events, the seismic moment can be usually determined from body waves. For these small earthquakes, the shape of the fault plane is not known so that a simple circular fault model with radius r is often used. If the source is simple, the pulse width τ is approximately equal to r/V_r. Since $V_r \approx 0.7\beta$, $\tau = c_2 r/\beta$, where c_2 is a constant of the order of 1 (Geller 1976, Cohn et al 1982). Another way of determining the source dimension is to use the frequency spectrum of seismic waves. Brune (1970) related the corner frequency f_0 of the S wave spectrum to r. Theoretically, if the source is simple, the pulse width τ can be translated to a corner frequency f_0, but if the source is complex, the interpretation of f_0 is not straightforward. Because of its simplicity, this method is widely used. However, many assumptions were built into this method (e.g. circular fault etc), so that the values determined for individual events are subject to large uncertainties, but the average of many determinations is considered significant.

Method 5 is most straightforward in concept, but is difficult to use unless high-quality data are available, preferably in both near- and far-field. With the increased availability of strong-motion records, this method is now widely used (e.g. Hartzell & Helmberger 1982). The slip function on the fault plane is determined directly, which can be used to estimate not only the average stress drop but also local stress drop.

Many determinations of stress drops have been made by combining these methods. Figure 6*a* shows the relation between M_0 and S for large and great earthquakes (Kanamori & Anderson 1975). In general, log S is proportional to (2/3) log M_0. Since $M_0 = \mu SD = c\Delta\sigma S^{3/2}$, Figure 6*a* indicates that $\Delta\sigma$ is constant over a large range of M_0. The straight lines in Figure 6*a* show the trends for circular fault models with $\Delta\sigma = 1$, 10, and 100 bars. The actual value of the stress drop depends on the fault geometry and other details, but the overall trend appears well established. Stress drop $\Delta\sigma$ varies from 10 to 100 bars for large and great earthquakes.

For smaller earthquakes, it is necessary to use higher frequency waves to determine source dimensions, but the strong attenuation and scattering of high-frequency waves make the determination of source dimensions more difficult. Because of this difficulty, whether the trend shown in Figure 6*a* continues to very small source dimensions or not has been debated. Several studies indicate that it breaks down at $r = 100$ m, but a recent result obtained by Abercrombie & Leary (1993) from down-hole (2.5 km) observations near Cajon Pass, California, suggests that the trend continues to at least $r = 10$ m, as shown in Figure 6*b*.

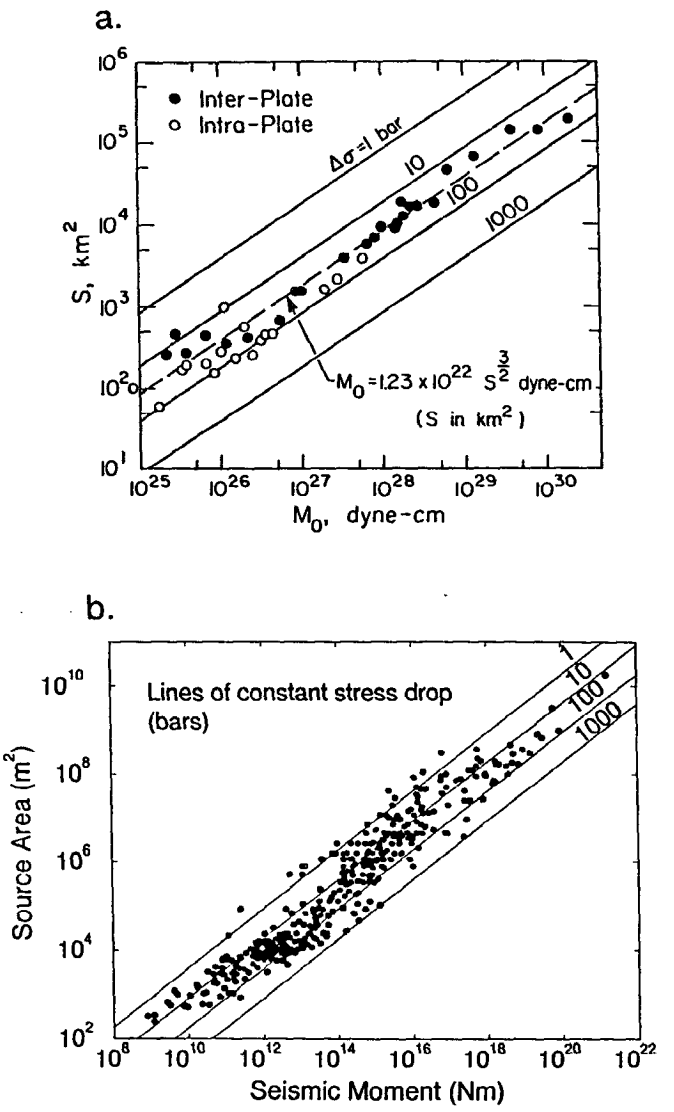

Figure 6 (*a*) Relation between fault area S and seismic moment M_0, for large and great earthquakes (Kanamori & Anderson 1975). (*b*) Relation between seismic moment M_0 and source area for small and large earthquakes (Abercrombie & Leary 1993).

These results suggest that $\Delta\sigma$ averaged over a distance of 100 m or longer appears to be within a range of 1 to 1000 bars, for a range of M_0 from 10^{16} to 10^{30} dyne-cm. The implications of the constant stress drop have been discussed by many investigators (e.g. Aki 1971, Hanks 1979).

High Stress-Drop Events

As shown in Figures 6*a* and 6*b*, the static stress drops of most large ($M > 5.5$ or $M_0 > 2.2 \times 10^{24}$ dyne-cm) earthquakes are in the range of 10 to 100 bars, but there are some exceptions. Moderate earthquakes with very high stress drops (300 bars to 2 kbars) are occasionally observed. For example, Munguia & Brune (1984) found very high stress-drop (up to 2.5 kbars) earthquakes in the area of the 1978 Victoria, Baja California, earthquake swarm. These earthquakes are characterized by high-frequency source spectra. To identify these high stress-drop earthquakes, near-field observations are necessary. As the distance increases, the attenuation of high-frequency energy makes it difficult to identify high stress-drop earthquakes.

Recently several high stress-drop earthquakes were observed with close-in wide-dynamic range seismographs. For example, Kanamori et al (1990, 1993) estimated $\Delta\sigma$ of the 1988 Pasadena, California, earthquake ($M = 4.9$) to be 300 bars to 2 kbars over a source dimension of about 0.5 km. Another example is the 1991 Sierra Madre, California, earthquake ($M = 5.8$). Wald (1992) and Kanamori et al (1993) estimated $\Delta\sigma$ to be 150 to 300 bars over a source dimension of about 4 km. The large range given to these estimates is due to the uncertainty in the source dimension and rupture geometry. Nevertheless, there is little doubt that these earthquakes have a significantly larger stress drop than most earthquakes. These results indicate that $\Delta\sigma$ can be very large over a scale length of a few km. In most large earthquakes, regions of high and low stress drops are averaged out resulting in $\Delta\sigma$ of 10 to 100 bars.

Although these high stress-drop earthquakes may occur only in special tectonic environments, we consider that they represent an end-member of earthquake fault models, as we discuss later.

Dynamic Stress Drop

As discussed earlier, the dynamic stress drop $\Delta\sigma_d$ is the stress that drives fault motion, and controls the particle velocity of fault motion. The particle velocity $\dot{U}$ of fault motion is thus an important seismic source parameter that provides estimates of $\Delta\sigma_d$, through relations like (2) or (5).

Maximum ground motion velocities recorded by strong motion instruments provide crude estimates of the particle velocity of fault motion. Brune (1970) suggested, using the data from six earthquakes, an upper

limit of the particle velocity of 1 m/sec. A compilation of strong-motion data by Heaton et al (1986, figure 20) also indicates that the upper limit of the observed ground motion velocity is about 1 m/sec.

Unfortunately, direct determination of $\dot{U}$ is not very easy because the observed waveform is the convolution of the local dislocation function and the fault rupture function. Kanamori (1972) estimated $\dot{U}$ for the 1943 Tottori, Japan, earthquake to be about 42 cm/sec using a very simple fault model. A similar method was used to determine the particle velocities for several Japanese earthquakes: 1 m/sec for the 1948 Fukui earthquake (Kanamori 1973), 50 cm/sec for the 1931 Saitama earthquake (Abe 1974a), 30 cm/sec for the 1963 Wakasa Bay earthquake (Abe 1974b), and 92 cm/sec for the 1968 Saitama earthquake (Abe 1975). These results indicate a range of $\Delta\sigma_d$ from 40 to 200 bars (using 2) and 20 to 100 bars (using 5). Boatwright (1980) developed a method to determine dynamic stress drops from seismic body waves.

Some eyewitness reports suggest somewhat larger particle velocities, but even if we allow for the uncertainties in the measurements, $\dot{U}$ appears to be bounded at about 2 m/sec.

For more recent earthquakes, the distribution of slip and particle velocity is determined by seismic inversion. Heaton (1990) estimated $\Delta\sigma_d$ for several earthquakes from the particle motion velocities thus determined. His estimate ranges from 12 to 40 bars for the average $\Delta\sigma_d$, and from 22 to 84 bars for the local $\Delta\sigma_d$.

Quin (1990) and Miyatake (1992a,b) attempted to determine $\Delta\sigma_d$ from the slip time history estimated by seismic inversion. Quin (1990) modeled the dynamic stress release pattern of the 1979 Imperial Valley, California, earthquake using the slip distribution determined by Archuleta (1984). Miyatake (1992a,b) used the slip models for the Imperial Valley earthquake and several Japanese earthquakes determined by Takeo (1988) and Takeo & Mikami (1987), and estimated the static stress drop $\Delta\sigma$ on the fault plane from the slip distribution. Assuming that $\Delta\sigma_d = \Delta\sigma$, he computed the local slip function using the method developed by Mikumo et al (1987). A good agreement between the computed slip function and that determined by seismic inversion led him to conclude that $\Delta\sigma_d \approx \Delta\sigma$ (within a factor of 2), which is in good agreement with Quin's (1990) result. Since the rise time of local slip function determined by seismic inversion is usually considered to be the upper limit (a very short rise time cannot be resolved with the available seismic data), the conclusion by Quin and Miyatake indicates that $\Delta\sigma_d$ is comparable to $\Delta\sigma$, or possibly larger. However, $\Delta\sigma_d$ is unlikely to be much higher than 200 bars, because the observed particle velocity seems to be bounded at about 2 m/sec.

McGuire & Hanks (1980) and Hanks & McGuire (1981) related the

root-mean-square (RMS) acceleration to stress drop. Using this relation, Hanks & McGuire (1981) estimated stress drops for many California earthquakes to be about 100 bars. This estimate, obtained from the radiated wave field rather than the static field, can be regarded as a measure of the average $\Delta\sigma_d$.

In summary, $\Delta\sigma_d$ varies over a range of 20 to 200 bars, which is approximately the same as that for $\Delta\sigma$.

Asperities and Barriers

Many studies have shown that slip distribution on a fault is very complex, i.e. most large earthquakes are multiple events at least on a time scale of a few seconds to a few minutes (e.g. Imamura 1937, Miyamura et al 1964, Wyss & Brune 1967, Kanamori & Stewart 1978). Recent seismic inversion studies have shown this complexity in great detail for earthquakes in both subduction zones (e.g. Ruff & Kanamori 1983; Lay et al 1982; Beck & Ruff 1987, 1989; Schwartz & Ruff 1987; Kikuchi & Fukao 1987) and in continental crusts (see Heaton 1990 for a summary). Two examples are shown in Figure 7 (Wald et al 1993, Mendoza & Hartzell 1989).

These models have been often interpreted in terms of *barriers*—areas where no slip occurs during a main shock (Das & Aki 1977), and *asperities*—areas where large slip occurs during a main shock (e.g. Kanamori 1981). The mechanical properties of the areas between asperities are poorly understood. One possibility is that the slip there occurs gradually in the form of creep and small earthquakes during the interseismic periods. If this is the case, the same asperities break in every earthquake cycle, producing a "characteristic" earthquake sequence. Another possibility is that the areas between asperities remain locked (i.e. barriers) until the next major sequence when they fail as asperities for that sequence. In this case, the rupture pattern would be very different from sequence to sequence resulting in a "noncharacteristic" earthquake sequence. It is also possible that asperities and barriers are not permanent features, but are controlled by nonlinear frictional characteristics so that the distribution of asperities and barriers can vary in a chaotic fashion (Rice 1991). The distributions of barriers and asperities could also change due to redistribution of water and pore pressure before and during earthquakes.

Since the physical nature of asperities and barriers is not well understood, here we use the terms simply to describe complexity of fault rupture patterns. Regardless of their physical nature, it is important to recognize that the mechanical properties (strength and frictional characteristics) of fault zones are spatially very heterogeneous and the degree of heterogeneity varies significantly for different fault zones.

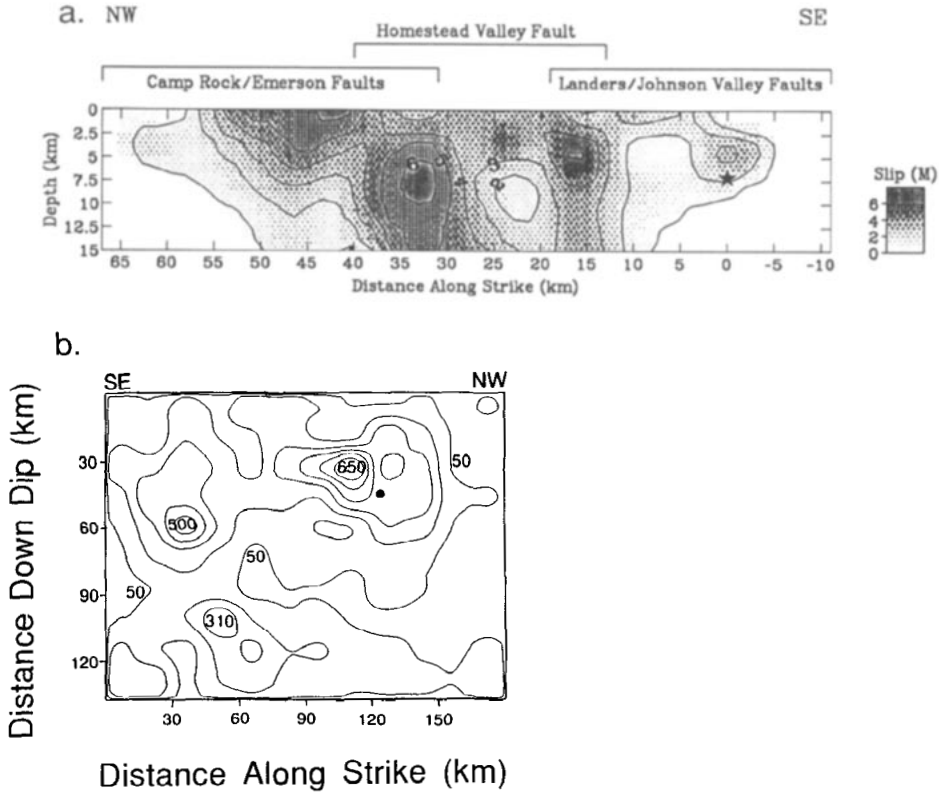

Figure 7 (*a*) Rupture pattern of the 1992 Landers, California, earthquake determined from strong-motion, teleseismic, and geodetic data (after Wald & Heaton 1993). (*b*) Rupture pattern of the 1985 Michoacan, Mexico, earthquake determined from strong-motion and teleseismic data (after Mendoza & Hartzell 1989). In both (*a*) and (*b*), the contour lines show the total amount of displacement. In these studies, in addition to displacements, slip velocities are also approximately determined.

Energy Release

Since energy release in an earthquake is caused by fault motion driven by dynamic stress, the energy budget of an earthquake must provide a clue to the stress change during an earthquake. The simplest way to investigate this problem is to consider a crack in an elastic medium on which the stress drops from σ_0 to σ_1. During slippage frictional stress acts against motion. This type of intuitive model was first used by Orowan (1960), and has been subsequently used by many investigators (Savage & Wood 1971, Wyss & Molnar 1972).

The total energy change is then given by

$$W = \tfrac{1}{2}S(\sigma_0+\sigma_1)\bar{D} = S\bar{\sigma}\bar{D}, \tag{8}$$

where S is the surface area of the crack, $\bar{\sigma}$ is the average stress, and $\bar{D}$ is the displacement averaged over the crack surface (Knopoff 1958, Kostrov 1974, Dahlen 1977, Savage & Walsh 1978).

Since slip occurs against frictional stress σ_f, the energy $H = \sigma_f S\bar{D}$ will be lost to heat. If we ignore the energy necessary to create new surfaces at the crack tip (surface energy), we can assume that the difference will be radiated by elastic waves. Thus

$$E_S = W - H. \tag{9}$$

The importance of surface energy has been discussed by Husseini (1977) and Kikuchi & Fukao (1988). In general, if $V_r/\beta = 0.7$ to 0.8, the surface energy is about 1/4 of E_S (Husseini 1977), so that the radiated energy is about 3/4 of the E_S given by (9). Kikuchi & Fukao (1988) showed that this ratio also depends on the aspect ratio of the fault, and in an extreme case, the radiated energy can be only 10% of the E_S given by (9). Considering the limited accuracy of the energy estimate, we will ignore the surface energy in the following discussion. However, the surface energy could be important under certain circumstances.

The relations (8) and (9) are most conveniently illustrated in Figure 8 which was used by Kikuchi & Fukao (1988) and Kikuchi (1992). The vertical axis is the stress on the fault plane (crack surface) and the horizontal axis is the displacement measured in $S\bar{D}$. The total energy release W is given by the trapezoid OABC (Equation 8). In the simplest case (Case I) we assume that $\sigma_f = \text{const}$ and $\sigma_1 = \sigma_f$, i.e. the shear stress on the fault after an earthquake is equal to σ_f. In this case heat loss $H = \sigma_f S\bar{D}$ is given

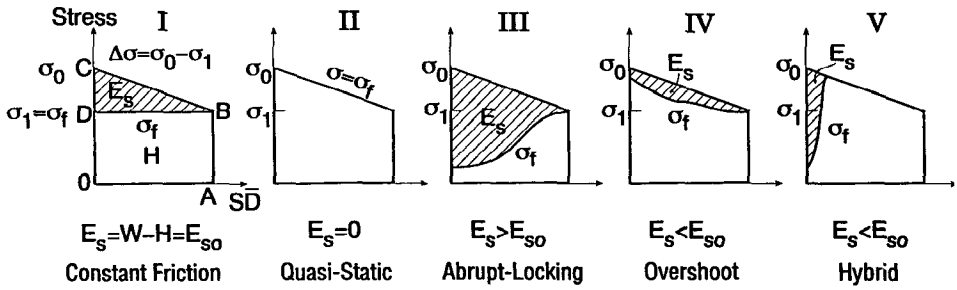

Figure 8 Schematic representation of energy budget for a stress relaxation model (modified from Kikuchi & Fukao 1988). Case I: Constant Friction model; Case II: Quasi-Static model; Case III: Abrupt-Locking model; Case IV: Overshoot model; Case V: Hybrid model.

by the rectangular area OABD, and E_S is given by the triangular area DBC. Thus

$$E_S = W - H = \tfrac{1}{2}S\bar{D}[(\sigma_0+\sigma_1)-2\sigma_f] = \tfrac{1}{2}S\bar{D}[(\sigma_0-\sigma_1)-2(\sigma_f-\sigma_1)]. \quad (10)$$

If we assume $\sigma_1 = \sigma_f$, then the second term in the brackets vanishes, and (10) is reduced to

$$E_S = \tfrac{1}{2}S\bar{D}(\sigma_0-\sigma_1) = \frac{\Delta\sigma}{2\mu}M_0. \quad (11)$$

Since both M_0 and $\Delta\sigma$ can be determined with seismological methods, the radiated energy E_S can be estimated using (11). Kanamori (1977) used this relationship to estimate the amount of energy released by large earthquakes. Although no direct evidence is available for the validity of the assumption $\sigma_1 = \sigma_f$, the relation (11) seems to hold for many large earthquakes for which M_0 and E_S have been independently estimated. However, since many assumptions and simplifications have been made in obtaining (11), E_S thus estimated should be considered only approximate.

It is useful to consider a few alternatives using the diagrams shown in Figure 8. The most extreme is a quasi-static case (Case II in Figure 8) in which frictional stress is adjusted so that it is always equal to the stress on the fault plane. In this case the frictional stress is given by the straight line CB, and no energy is radiated (i.e. $E_S = 0$). The entire strain energy is expended to generate heat and to create new crack surfaces. The other extreme case (Case III in Figure 8) involves a sudden drop in friction, possibly at the time slippage begins. In this case a larger stress is available for driving the fault motion, and more seismic energy will be radiated than in Case I. Case IV in Figure 8, which is intermediate between Case I and Case II, represents less wave energy radiation than Case I. Kikuchi & Fukao (1988) and Kikuchi (1992), using the data on E_S, M_0, and $\Delta\sigma$, favored this case. In this case the contribution of surface energy is important. The dynamic stress drop during faulting, $\sigma-\sigma_f$, is smaller than the static stress drop $\Delta\sigma$. It is also possible that dynamic stress can be very large during a short period of time, but then drops quickly to a low level so that E_S is smaller than that for Case I. This is shown as Case V in Figure 8. In Figure 8 the large $\Delta\sigma_d$ occurs at the beginning, but it can happen at any time during faulting.

These models are useful for understanding the basic behavior of complex earthquake faulting. However, because actual fault zones may be very different, both between different tectonic provinces (e.g. subduction zones, transform faults, intra-plate faults, etc) and between faults with different characteristics in the same province (e.g. faults with slow slip rate vs fast

slip rate, etc), it is likely that more than one of the mechanisms discussed above are involved in real faulting.

As shown by Figure 8 and Equation (11), the ratio $2\mu E_S/M_0$ gives a measure of the average dynamic stress drop $\Delta\sigma_d$ during slippage. If $\sigma_f = \text{const}$ and $\sigma_1 = \sigma_f$ (Case I), then $\Delta\sigma_d = \Delta\sigma$. However, for Cases III, IV and V,

$$2\mu\frac{E_S}{M_0} = \Delta\sigma_d = \eta_S\Delta\sigma, \tag{12}$$

when $\eta_S > 1$ for Case III and $\eta_S < 1$ for Cases IV and V.

Unfortunately, estimating energy E_S is not easy. Traditionally, E_S has been estimated from the earthquake magnitude M. The most commonly used relation is the Gutenberg-Richter relation (Gutenberg & Richter 1956):

$$\log E_S = 1.5M_S + 11.8 \quad (E_S \text{ in ergs}),$$

where M_S is the surface-wave magnitude. However, this is an average empirical relation, and is not meant to provide an accurate estimate of E_S. The total energy must be estimated by an integral of the entire wave train, rather than from M_S which is determined by the amplitude at a single period of 20 sec.

Currently, radiated energy is estimated directly from seismograms. Two methods are being used. In the first method (Thatcher & Hanks 1973, Boatwright 1980, Boatwright & Choy 1985, Bolt 1986, Houston 1990a,b), the ground-motion velocity of radiated waves, either body or surface waves, is squared and integrated to estimate E_S. Sometimes equivalent computation is done on the frequency domain. In this method, the major difficulties are obtaining complete coverage of the focal sphere and in the correction of the propagation effects, i.e. geometrical spreading, attenuation, waveguide effects, and scattering. If a large amount of data is available, one can estimate E_S fairly accurately with several empirical corrections and assumptions.

The second method involves determination of the source function by inversion of seismograms (Vassiliou & Kanamori 1982, Kikuchi & Fukao 1988). In this case, the propagation effects are removed through the process of inversion, but the solution is usually band-limited in frequency. Nevertheless, with the advent of sophisticated inversion algorithms, this method has been used with considerable success (Kikuchi & Fukao 1988).

Kanamori et al (1993) estimated E_S using the high-quality broadband data that has recently become available at short distances from earth-

quakes in southern California. Figure 9 shows the relation between E_S and M_0 thus obtained for recent earthquakes in southern California. The dynamic stress drops shown in Figure 9 are computed using (12) with $\mu = 3 \times 10^{11}$ dynes/cm^2. The earthquakes shown in Figure 9 [the 1989 Montebello earthquake ($M = 4.6$), the 1988 Pasadena earthquake ($M = 4.9$), the 1991 Sierra Madre earthquake ($M = 5.8$), the 1992 Joshua Tree earthquake ($M = 6.1$), the 1992 Big Bear earthquake ($M = 6.4$), and the 1992 Landers earthquake ($M = 7.3$)] have stress drops in a range of 50 to 300 bars—significantly higher than those for many large earthquakes elsewhere computed by Kikuchi & Fukao (1988) from the E_S/M_0 ratios. As will be discussed later, this difference can be interpreted as due to the long repeat times of the earthquakes shown in Figure 9.

The values of $\Delta\sigma_d$ shown in Figure 9 are smaller than $\Delta\sigma$ for the same earthquakes (not shown here; see Kanamori et al 1993) by a factor of about 3. Kikuchi & Fukao (1988) found an even larger difference for the earthquakes they examined. They attributed this difference to surface energy, and favored the Case IV stress release model shown in Figure 8. However, estimates of $\Delta\sigma_d$ and $\Delta\sigma$ are subject to large uncertainties so that whether this difference is significant or not is presently unresolved.

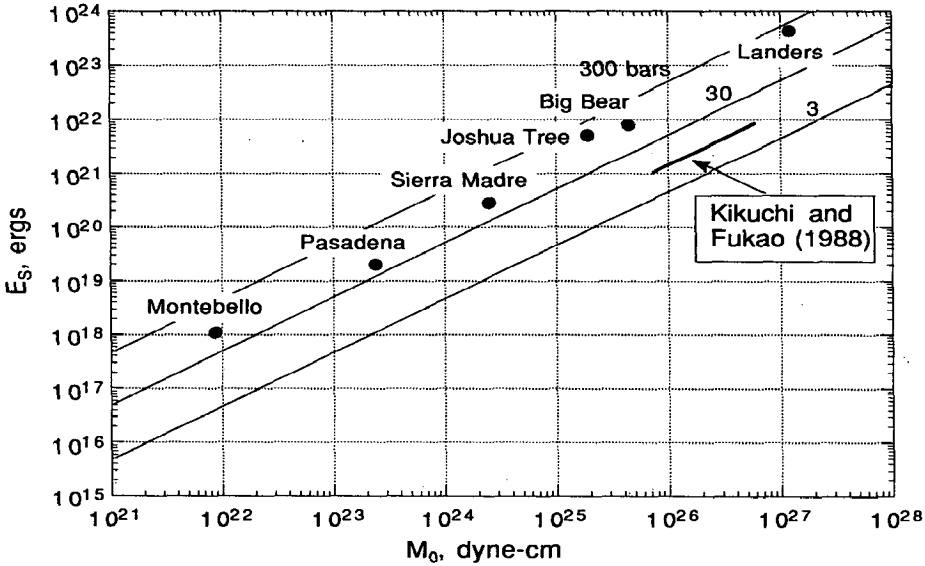

Figure 9 The relation between seismic moment M_0 and energy E_S. The heavy solid line indicates the range of the E_S/M_0 ratios of large earthquakes determined by Kikuchi & Fukao (1988).

Relationship between Stress Drop and Slip Rate

The slip rate of faults varies significantly from less than 1 mm/year to several cm/year. Faults with slow and fast slip rates usually have long and short repeat times, respectively. Kanamori & Allen (1986) and Scholz et al (1986) independently found that earthquakes on faults with long repeat times radiate more energy per unit fault length than those with short repeat times. Houston (1990b) also found evidence for this. Figure 10 shows the results obtained by Kanamori & Allen (1986). A typical earthquake on a fault with fast slip rate and short repeat time is the 1966 Parkfield, California, earthquake ($M = 6$, slip rate = 3.5 cm/year, repeat time = 22 years). In contrast, a typical earthquake on a fault with slow slip rate is the 1927 Tango, Japan, earthquake ($M = 7.6$, repeat times > 2000 years). Even if the Tango earthquake has about the same fault length as the Parkfield earthquake, its magnitude is more than 1.5 units larger. A more recent example is the 1992 Landers, California, earthquake. Despite the relatively large magnitude, its fault length is only 70 km. The repeat time

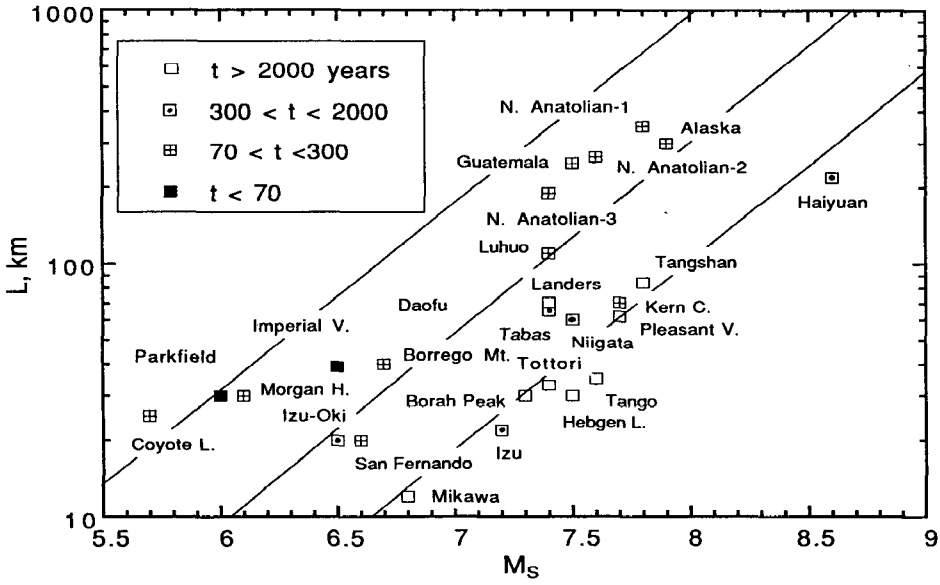

Figure 10 Relation between fault length L and surface-wave magnitude M_S (modified from Kanamori & Allen 1986). The fault length is shorter for earthquakes with long repeat times than for those with short repeat times with the same M_S. Since the energy released E_S is proportional to $10^{1.5M_S}$, the above relation means that earthquakes on faults with long repeat times radiate more energy per unit fault length than those with short repeat times.

of the Landers earthquake is believed to be very long (see below). As shown in the previous section, a larger amount of energy release per unit fault length suggests a larger dynamic stress drop. Thus, this observation suggests that dynamic stress drop increases as fault slip rate decreases.

The implication is that the strength of a fault increases with the time during which the two sides of the fault have been locked. This may be viewed as manifestation of an evolutionary process of a fault (Scholz 1989).

The results for the E_S/M_0 ratio shown in Figure 9 can be interpreted in the same way. The repeat time of major earthquakes on the frontal fault system where the Pasadena and the Sierra Madre earthquakes occurred is believed to be very long—a few thousand years (e.g. Crook et al 1987). Also, the repeat time of the faults in the eastern Mojave desert where the Joshua Tree, the Big Bear, and the Landers earthquakes occurred is thought to be very long (e.g. Sieh et al 1993). Since no measurements of E_S/M_0 have been made yet for earthquakes on faults with short repeat times in southern California, we cannot directly compare $\Delta\sigma_d$ for earthquakes with long and short repeat times in southern California. Nevertheless, Figure 9 provides evidence that earthquakes with long repeat times have larger dynamic stress drops.

STRESS RELEASE MODELS FOR EARTHQUAKES

Housner (1955) and Brune (1970) presented a model in which only part of the total available stress is released during an earthquake. Partial stress drop could be caused by some obstacles (e.g. interlocking asperities) prematurely stopping fault motion. Brune (1976) later called this the abrupt-locking model. An important consequence of this model is a significantly larger dynamic stress drop than static stress drop.

Many abrupt-locking mechanisms can be considered. Fault rupture may encounter a strong spot on the fault which prevents the fault from rupturing further. Another possibility is that rapid healing of the rupture surface during slippage, which slows down the particle motion of the fault, eventually brings it to a halt. Rapid healing results in a change of kinetic friction, which plays a key role in controlling slip behavior (Dieterich 1979, Scholz 1989). For most materials, kinetic friction is considerably smaller than static friction (Bowden & Taber 1964, Rabinowicz 1965); a power law of the form, $\sigma_f = av^{-b}$ (v = sliding velocity, a and b = constants), is often used in material science.

Many mechanisms for the reduction of kinetic friction have been suggested, for example: 1. melting on the fault plane, 2. acoustic fluidization (Melosh 1979), 3. infinitesimal motion normal to the slip plane (Schallamach 1971, Brune et al 1993). Since most experimental data on dynamic

friction have been obtained for sliding velocities much lower than those present during seismic faulting, about 1 m/sec, the exact behavior of kinetic friction in real fault zones can only be assumed.

Heaton (1990), recognizing that the duration of slip at a given point on a fault is much shorter than the duration of rupture over the entire fault, attempted to explain this observation using a velocity-dependent kinetic friction law ($\sigma_f = \sigma_{f_0} - c\dot{D}$, c = constant). As shown in Figure 5*b*, a crack tip causes the square-root stress singularity ahead of the rupture front. Just behind the rupture front the fault particle velocity becomes very high, thus decreasing kinetic friction. As the particle velocity decreases away from the crack tip, kinetic friction increases again, and the fault motion eventually stops. Thus, at a given time during faulting, slip is occurring over a short distance (slip pulse). This slip pulse propagates on a fault at the rupture velocity. Heaton (1990) called this model the "slip-pulse model." In the slip-pulse model, it is the velocity-dependent kinetic friction rather than the static stress near the fault that controls dynamic fault motion.

Brune et al (1993) found evidence for fault-normal motion during slippage in their foam rubber models of rupture. The fault-normal motion can effectively reduce the normal stress which in turn reduces kinetic friction during slippage.

The energy release pattern for the abrupt-locking model or slip-pulse model can be represented by Case III or Case V in Figure 8.

The details of the frictional characteristics are still unknown, and a better understanding of kinetic friction during slippage under the conditions that prevail during seismic faulting [high normal stress, high (1 m/sec) particle velocity, etc] is critically important for understanding the physics and mechanics of earthquake faulting.

MODELS FOR HETEROGENEOUS FAULTS

As summarized in the previous sections, any model for earthquake process must take into account the following:

1. The static stress drop $\Delta\sigma$ is, on the average, 1 to 100 bars. Some events, however, have very high stress drops.
2. The dynamic stress drop $\Delta\sigma_d$ is, on the average, about the same order as the static stress drop $\Delta\sigma$. However, it may vary significantly as a function of time and space, and could exceed the static stress drop for a short period of time during faulting. In general, both dynamic and static stress drops appear to be higher for faults with slow slip rates (long repeat times) than those with fast slip rates (short repeat times).
3. The slip distribution on a fault plane is generally very complex, sug-

gesting heterogeneity in the strength or frictional characteristics of the material in the fault zone.

End-Member Models

To understand the complexity of fault rupture patterns, we first consider simple end-member models characterized by different magnitudes of $\Delta\sigma_d$ and $\Delta\sigma$.

Table 1 summarizes four end-member models thus introduced. In this table "high" and "low" typically mean 300 and 30 bars, respectively, but they are meant to be representative values. Type 1 has high $\Delta\sigma_d$ and high $\Delta\sigma$, and is a model for small to moderate size earthquakes on a fault with slow slip rate, such as the 1988 Pasadena, the 1991 Sierra Madre, and the 1992 Landers earthquakes. Type 2 has high $\Delta\sigma_d$ and low $\Delta\sigma$. This is essentially the abrupt-locking partial stress-drop model (Brune 1970, 1976) and the slip-pulse model (Heaton 1990). Fault slip motion occurs very rapidly, but it locks up prematurely by either encountering an obstacle or sudden healing. Type 3 has low $\Delta\sigma_d$ and high $\Delta\sigma$. This corresponds to the overshoot model described by Madariaga (1976). The model suggested by Kikuchi & Fukao (1988) and Kikuchi (1992) belongs to this type in which the effective driving stress is smaller than the static stress drop. The most extreme case of this type would be creep. If the sliding condition is such that kinetic friction is always equal to shear traction on the fault plane, the fault motion becomes quasi-static without seismic radiation. Type 4 has both low $\Delta\sigma_d$ and low $\Delta\sigma$. Variations of pore pressures (Sibson 1973, Rice 1992), rock types (Allen 1968), fault geometry (Sibson 1986), and chemical process may be responsible for these different types of faults.

Composite Models

Evidence for abrupt-locking and slip-pulse models has been discussed by Heaton (1990) and Brune (1991). Brune et al (1986) presented many examples of ω^{-1} roll-off of the source spectrum which suggests partial stress drop. Heaton (1990) presented examples of slip-pulse ruptures. For

Table 1 Four end-member models

	$\Delta\sigma_d$	$\Delta\sigma$	$\dot{U}$	U^a
Type 1	high	high	large	large
Type 2	high	low	large	small
Type 3	low	high	small	large
Type 4	low	low	small	small

[a] A uniform scale length is assumed.

these models, $\Delta\sigma_d$ must be significantly larger than $\Delta\sigma$. The results of Quin (1990) and Miyatake (1992a,b), however, show $\Delta\sigma_d \approx \Delta\sigma$. It is possible that $\Delta\sigma_d$ determined in these inversion studies is a lower bound because of the limited resolution of the method. Kikuchi & Fukao (1988) and Kikuchi (1992) favor the Case IV energy release pattern (Figure 8) which is not consistent with the partial stress-drop model or slip-pulse model. However, Case V which is a modification of Case IV can probably satisfy the data presented by Kikuchi & Fukao (1988) and Heaton (1990).

As discussed earlier, actual earthquake sequences are extremely complex, and are likely to involve more than one mechanism. In view of this complexity, we now try to interpret earthquake sequences using combinations of the end-member models described above.

Figure 11*a* shows a combination of Type 1 and Type 4 behavior. Since $\Delta\sigma_d$ and $\Delta\sigma$ are directly proportional to particle velocity $\dot{U}$ and displacement U, respectively, the variations of $\dot{U}$ and U along the fault will be as schematically shown in Figure 11*a*. This combination explains the rupture patterns of the 1979 Imperial Valley earthquake (Quin 1990, Miyatake 1992a) for which $\Delta\sigma_d \approx \Delta\sigma$. Other earthquakes such as the 1984 Morgan Hills, California, earthquake (Hartzell & Heaton 1986, Beroza & Spudich 1988), the 1987 Superstition Hills, California, earthquake (Wald et al 1990), and the 1989 Loma Prieta, California, earthquake (e.g. Hartzell et al 1991, Wald et al 1991, Steidl et al 1991, Beroza 1991) probably belong to this category.

If we have a combination of Type 1 and Type 2 behavior, $\dot{U}$ and U may appear as shown in Figure 11*b*. In this case, an abrupt-locking or slip-

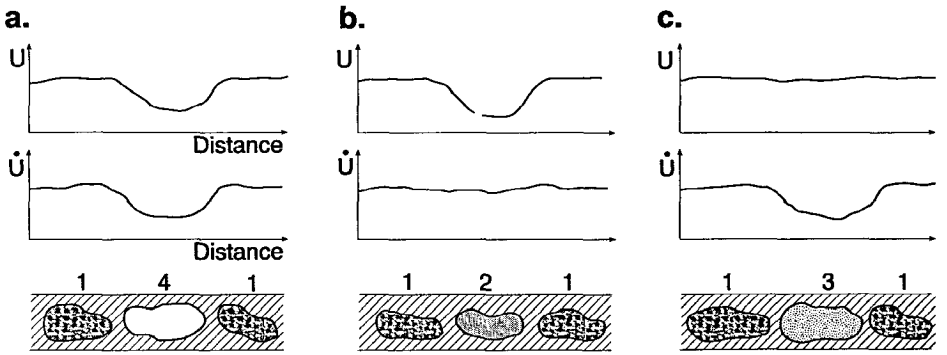

Figure 11 Composite fault models. (*a*) Combination of Type 1 (high $\Delta\sigma_d$ and high $\Delta\sigma$) and Type 4 (low $\Delta\sigma_d$ and low $\Delta\sigma$). Schematic distributions of slip and slip velocity are shown. (*b*) Combination of Type 1 and Type 2 (high $\Delta\sigma_d$ and low $\Delta\sigma$). (*c*) Combination of Type 1 and Type 3 (low $\Delta\sigma_d$ and high $\Delta\sigma$).

pulse mechanism must prevail over a significant section of the fault. The results obtained by Quin (1990) and Miyatake (1992a,b) do not exhibit this pattern. However, as T. Heaton (personal communication, 1993) suggests, if the rise time determined by inversion is the upper bound, then this combination represents the rupture patterns of earthquakes mentioned above. In any event, for these combinations the low and high static-stress drops are averaged out to yield the moderate static-stress drop typical of crustal earthquakes occurring on active plate boundaries.

The combination of Type 1 and Type 3 models would yield a pattern as shown in Figure 11*c*. The slip would be relatively large and uniform over the entire fault, but the slip velocity is high only at limited places. This could be a model for the 1906 San Francisco, California, earthquake. Wald et al (1993) concluded that relatively short-period (20 sec or less) seismic waves were excited from a fault segment about 100 km long, while the geodetic data and the surface break indicate fairly uniform slip over a distance of 350 km (Thatcher 1975). Although no direct seismic data are available, the 1857 Fort Tejon, California, earthquake had a relatively uniform and large slip over 350 km (Sieh 1978), and could be of this type. The creeping section of the San Andreas fault north of the 1857 rupture zone is the extreme Type 3 case.

Three other combinations can be made, but the two end-member models (Type 1 for high stress-drop earthquakes and Type 3 for creep events) and the three combinations described above seem to explain the important features of most earthquake sequences.

CONCLUSION

Fault Strength

The particle velocity of fault motion appears to be bounded at about 1 to 2 m/sec which corresponds to an upper bound of $\Delta\sigma_d$ of about 100 to 200 bars (Equation 5). The values of $\Delta\sigma_d$ determined from the E_S/M_0 ratios (Figure 9) support this. Thus, if σ_f is bounded at 200 bars, as suggested by the heat flow arguments, then, considering the observation $\Delta\sigma_d \approx \Delta\sigma$, the strength of fault σ_0, defined in Figure 1, cannot be much higher than 400 bars. A corollary of this is that the strength of the crust varies significantly. As Jeffreys (1959) showed, the existence of high mountains such as the Himalayas indicates a large stress difference of at least 1.5 kbars within the outermost 50 km of the crust. Thus, although the strength of active fault zones such as the San Andreas is low, high stresses must be prevailing in the crust away from it. In other words, earthquakes occur where the crust is weak (Kanamori 1980, Zoback et al 1987). As mentioned earlier, some earthquakes on faults with low slip rates tend to have high stress

drops. Since the slip rates are low, these earthquakes would not produce a significant heat flow anomaly even if the stress drop is high.

The above argument hinges on the premise that the lack of heat flow anomaly indicates low kinetic friction during faulting. If the heat flow problem can be interpreted differently (e.g. Scholz 1992), however, the above conclusion must be modified significantly.

Static Stress Drop vs Dynamic Stress Drop

The values of $\Delta\sigma_d$ obtained from particle velocities of fault motion are, on the average, of the same order as $\Delta\sigma$. The available data of the E_S/M_0 ratio, however, suggest that the radiated energy E_S appears to be significantly less than expected for a simple model in which $\Delta\sigma_d \approx \Delta\sigma$. This appears to be inconsistent with the results obtained from slip and slip-velocity data. Since large uncertainties still exist in the estimates of any of these parameters, this difference may not be significant. However, if the difference is real, one way to explain it is to introduce a drastic time dependence of $\Delta\sigma_d$: $\Delta\sigma_d$ is very large only within a short time interval during faulting but decreases rapidly. This behavior is illustrated by the Case V energy release pattern shown in Figure 8, and is expected for the abrupt-locking or slip-pulse model. Iio (1992) found evidence for initial slow slip before the major fault motion, which suggests a rapid change in kinetic friction. Wald et al (1991) found evidence of a slow rupture about 2 sec before the main rupture of the 1989 Loma Prieta earthquake. These slow precursory events may be a manifestation of time-dependent kinetic friction during faulting, and merit further studies.

To resolve this problem completely, it would be necessary to determine the slip function on the fault plane and the energy release more accurately using broadband high-resolution data.

State of Stress on a Fault Plane

As many studies have demonstrated, the heterogeneity of mechanical properties along a fault inferred from the complexity of rupture patterns is probably one of the most important elements of earthquake faults. Since different segments may have drastically different strengths and frictional characteristics, it is necessary to consider different rupture mechanisms for different segments. When a rupture occurs over a long fault, different segments interact with each other in a complex fashion, thereby causing complex seismic radiation as observed.

Mechanical properties of faults may be controlled by many factors: lithology in the fault zone, temperature, pore pressure, fault geometry, fault orientation with respect to tectonic stress, and slip rates. Rupture initiation, propagation, and cessation are all controlled by the mechanical

properties of each segment. The overall rupture patterns in each seismic cycle (characteristic versus noncharacteristic) depend on how different fault segments interact with each other. A better understanding of these would require detailed studies of seismic radiation from earthquakes that occur in different tectonic environments. Because the quality of seismic data has dramatically improved recently, we can now determine the distribution of slip and particle velocity on a fault and the energy release during an earthquake much better than before. These improved data and the variations of these source parameters between earthquakes from different tectonic environments and from faults with different slip rates will provide an important clue to the mechanics of earthquakes.

ACKNOWLEDGMENTS

I benefited from discussions with Tom Heaton, Don Anderson, Masayuki Kikuchi, Takeshi Mikumo, Larry Ruff, and Dave Wald. This paper was built upon many hours of discussions during the Coffee Break of the Seismological Laboratory. I thank all the participants. This research was partially supported by the U.S. Geological Survey Grant 14-08-0001-G1774. This paper is Contribution No. 5214, Division of Geological and Planetary Sciences, California Institute of Technology.

Literature Cited

Abe K. 1974a. Seismic displacement and ground motion near a fault: the Saitama earthquake of September 21, 1931. *J. Geophys. Res.* 79: 4393–99

Abe K. 1974b. Fault parameters determined by near- and far-field data: The Wakasa Bay earthquake of March 26, 1963. *Bull. Seismol. Soc. Am.* 64: 1369–82

Abe K. 1975. Static and dynamic parameters of the Saitama earthquake of July 1, 1968. *Tectonophysics* 27: 223–38

Abercrombie R, Leary P. 1993. Source parameters of small earthquakes recorded at 2.5 km depth, Cajon Pass, Southern California: implications for earthquake scaling. *Geophys. Res. Lett.* 20: 1511–14

Aki K. 1971. Earthquake mechanism. *Tectonophysics* 13: 423–46

Aki K. 1979. Characterization of barriers on an earthquake fault. *J. Geophys. Res.* 84: 6140–48

Allen CR. 1968. The tectonic environment of seismically active and inactive areas along the San Andreas fault system. In *Proc. Conf. Geol. Probl. San Andreas Fault Syst.*, pp. 70–82. Palo Alto: Stanford Univ. Publ. Geol. Sci.

Archuleta RJ. 1984. A faulting model for the 1979 Imperial Valley earthquake. *J. Geophys. Res.* 89: 4559–85

Beck S, Ruff L. 1987. Rupture process of the great 1963 Kurile Islands earthquake sequence: asperity interaction and multiple event rupture. *J. Geophys. Res.* 92: 14,123–38

Beck S, Ruff L. 1989. Great earthquakes and subduction along the Peru trench. *Phys. Earth Planet. Int.* 57: 199–224

Beroza GC. 1991. Near-source modeling of the Loma Prieta earthquake: evidence for heterogeneous slip and implications for earthquake hazard. *Bull. Seismol. Soc. Am.* 81: 1603–21

Beroza GC, Spudich P. 1988. Linearized

inversion for fault rupture behavior: application to the 1984 Morgan Hill, California, earthquake. *Bull. Seismol. Soc. Am.* 78: 6275–96

Boatwright J. 1980. A spectral theory for circular seismic sources; simple estimates of source dimension, dynamic stress drop, and radiated seismic energy. *Bull. Seismol. Soc. Am.* 70: 1–27

Boatwright J, Choy GL. 1985. Teleseismic estimates of the energy radiated by shallow earthquakes. In *US Geol. Surv. Open File Rep.* 85-0290-*A*, *Workshop XXVIII on the Borah Peak, Idaho Earthquake*, ed. RS Stein, RC Bucknam, ML Jacobson, pp. 409–48. Menlo Park: US Geol. Surv.

Bolt BA. 1986. Seismic energy release over a broad frequency band. *Pageoph* 124: 919–30

Bowden FP, Tabor D. 1964. *The Friction and Lubrication of Solids*. Oxford: Clarendon. 374 pp.

Brace WF, Byerlee JD. 1966. Stick-slip as a mechanism for earthquakes. *Science* 153: 990–92

Brune JN. 1970. Tectonic stress and spectra of seismic shear waves from earthquakes. *J. Geophys. Res.* 75: 4997–5009

Brune JN. 1976. The physics of earthquake strong motion. In *Seismic Risk and Engineering Decisions*, ed. C Lomnitz, E Rosenblueth, pp. 141–71. New York: Elsevier

Brune JN. 1991. Seismic source dynamics, radiation and stress. *Rev. Geophys.* 29: 688–99 (Suppl.)

Brune JN, Brown S, Johnson PA. 1993. Rupture mechanism and interface separation in foam rubber models of earthquakes: A possible solution to the heat flow paradox and the paradox of large overthrusts. *Tectonophysics* 218: 59–67

Brune JN, Fletcher J, Vernon F, Haar L, Hanks T, Berger J. 1986. Low stress-drop earthquakes in the light of new data from the Anza, California telemetered digital array. In *Earthquake Source Mechanics*, ed. S Das, J Boatright, CH Scholz, pp. 237. 45. Washington, DC: Am. Geophys. Union

Brune JN, Henyey TL, Roy RF. 1969. Heat flow, stress, and the rate of slip along the San Andreas fault,California. *J. Geophys. Res.* 74: 3821–27

Burridge R. 1969. The numerical solution of certain integral equations with non-integrable kernels arising in the theory of crack prpagation and elastic wave diffraction. *Phil. Trans. R. Soc. London Ser. A* 265: 353–81

Byerlee JD. 1970. Static and kinetic friction of granite at high normal stress. *Inst. J. Rock Mech. Min. Soc.* 7: 577–82

Chen YT, Chen XF, Knopoff L. 1987. Spontaneous growth and autonomous contraction of a two-dimensional earthquake fault. *Tectonophysics* 144: 5–17

Chinnery MA. 1964. The strength of the Earth's crust under horizontal shear stress. *J. Geophys. Res.* 69: 2085–89

Cohn SN, Hong TL, Helmberger DV. 1982. The Oroville earthquakes: a study of source characteristics and site effects. *J. Geophys. Res.* 87: 4585–94

Crook RJ, Allen CR, Kamb B, Payne CM, Proctor RJ. 1987. Quaternary geology and seismic hazard of the Sierra Madre and associated faults, western San Gabriel Mountains. In *Recent Reverse Faulting in the Transverse Ranges, California, US Geol. Surv. Prof. Pap.* 1339, ed. DM Morton, RF Yerkes, pp. 27–64

Dahlen FA. 1977. The balance of energy in earthquake faulting. *Geophys. J. R. Astron. Soc.* 48: 239–61

Das S, Aki K. 1977. Fault planes with barriers: a versatile earthquake model. *J. Geophys. Res.* 82: 5658–70

Dieterich JH. 1979. Modeling of rock friction 2. Simulation of preseismic slip. *J. Geophys. Res.* 84: 2169–75

Freund L. 1979. The mechanics of dynamic shear crack propagation. *J. Geophys. Res.* 84: 2199–209

Geller RJ. 1976. Scaling relations for earthquake source parameters and magnitudes. *Bull. Seismol. Soc. Am.* 66: 1501–23

Gibowicz SJ. 1986. Physics of fracturing and seismic energy release: a review. *Pageoph* 124: 611–58

Griffith AA. 1920. The phenomena of rupture and flow in solids. *Phil. Trans. R. Soc. London Ser. A* 221: 169–98

Gutenberg B, Richter CF. 1956. Magnitude and energy of earthquakes. *Ann. Geofis. Rome* 9: 1–15

Hanks TC. 1979. b-value and w-g seismic source models: implications for tectonic stress variations along active crustal fault zones and the estimation of high-frequency strong ground motions. *J. Geophys. Res.* 84: 2235–42

Hanks TC, McGuire RK. 1981. The character of high-frequency strong ground motion. *Bull. Seismol. Soc. Am.* 71: 2075–95

Hanson ME, Sanford AR, Shaffer R. 1971. A source function for a dynamic bilateral brittle shear fracture. *J. Geophys. Res.* 76: 3375–83

Hartzell SH, Heaton TH. 1986. Rupture history of the 1984 Morgan Hill, California, earthquake from the inversion of strong motion records. *Bull. Seismol. Soc. Am.* 76: 649–74

Hartzell S, Helmberger DV. 1982. Strong-

motion modeling of the Imperial Valley earthquake of 1979. *Bull. Seismol. Soc. Am.* 72: 571–96
Hartzell S, Stewart GS, Mendoza C. 1991. Comparison of L1 and L2 norms in a teleseismic waveform inversion for the slip history of the Loma Prieta, California, earthquake. *Bull. Seismol. Soc. Am.* 81: 1518–39
Heaton T. 1990. Evidence for and implications of self-healing pulses of slip in earthquake rupture. *Phys. Earth Planet. Int.* 64: 1–20
Heaton T, Tajima F, Mori AW. 1986. Estimating ground motions using recorded accelerograms. *Surv. Geophys.* 8: 25–83
Henyey TL, Wasserburg GJ. 1971. Heat flow near major strike-slip faults in California. *J. Geophys. Res.* 76: 7924–46
Housner GW. 1955. Properties of strong ground motion earthquakes. *Bull. Seismol. Soc. Am.* 45: 197–218
Houston H. 1990a. Broadband source spectra, seismic energy, and stress drop of the 1989 Macquarie Ridge earthquake. *Geophys. Res. Lett.* 17: 1021 24
Houston H. 1990b. A comparison of broadband source spectra, scismic energies, and stress drops of the 1989 Loma Prieta and 1988 Armenian earthquakes. *Geophys. Res. Lett.* 17: 1413–16
Husseini MI. 1977. Energy balance for formation along a fault. *Geophys. J. R. Astron. Soc.* 49: 699–714
Ida Y. 1972. Cohesive force across the tip of a longitudinal-shear crack and Griggith's specific surface energy. *J. Geophys. Res.* 77: 3796–805
Ida Y, Aki K. 1972. seismic source time function of propagating longitudinal-shear cracks. *J. Geophys. Res.* 77: 2034–44
Iio Y. 1992. Slow initial phase of the P-wave velocity pulse generated by microearthquakes. *Geophys. Res. Lett.* 19: 477–80
Imamura A. 1937. *Theoretical and Applied Seismology*. Tokyo: Maruzen. 358 pp.
Jeffreys H. 1959. *The Earth*. Cambridge: Cambridge Univ. Press. 420 pp.
Kanamori H. 1972. Determination of effective tectonic stress associated with earthquake faulting. The Tottori earthquake of 1943. *Phys. Earth Planet. Int.* 5: 426–34
Kanamori H. 1973. Mode of strain release associated with major earthquakes in Japan. A. *Rev. Earth Planet. Sci.* 1: 213–39
Kanamori H. 1977. The energy release in great earthquakes. *J. Geophys. Res.* 82: 2981–87
Kanamori H. 1980. The state of stress in the Earth's lithosphere. In *Phys. Earth's Int., Course LXXVIII*, ed. AM Dziewonski, E Boschi, pp. 531–54. Amsterdam: North-Holland
Kanamori H. 1981. The nature of seismicity patterns before large earthquakes. In *Earthquake Prediction*, ed. DW Simpson, PG Richards, Maurice Ewing Ser. 4: 1–19. Washington, DC: Am. Geophys. Union
Kanamori H, Allen CR. 1986. Earthquake repeat time and average stress drop. In *Earthquake Source Mechanics, Geophys. Monogr.*, ed. S Das, J Boatwright, CH Scholz, pp. 227–35. Washington, DC: Am. Geophys. Union
Kanamori H, Anderson DL. 1975. Theoretical basis of some empirical relations in seismology. *Bull. Seismol. Soc. Am.* 65: 1073–95
Kanamori H, Hauksson E, Hutton LK, Jones LM. 1993. Determination of Earthquake Energy Release M_L Using TERRAscope. *Bull. Seismol. Soc. Am.* 83: 330–46
Kanamori H, Mori J, Heaton TH. 1990. The 3 December 1988, Pasadena earthquake ($M_L = 4.9$) recorded with the very broadband system in Pasadena. *Bull. Seismol. Soc. Am.* 80: 483–87
Kanamori H, Stewart G. 1978. Seismological aspects of the Guatemala earthquake of February 4, 1976. *J. Geophys. Res.* 83: 3427–34
Kikuchi M. 1992. Strain drop and apparent strain for large earthquakes. *Tectonophysics* 211: 107–13
Kikuchi M, Fukao Y. 1987. Inversion of long-period P-waves from great earthquakes along subduction zones. *Tectonophysics* 144: 231–47
Kikuchi M, Fukao Y. 1988. Seismic wave energy inferred from long-period body wave inversion. *Bull. Seismol. Soc. Am.* 78: 1707–24
Kikuchi M, Takeuchi H. 1971. Unsteady propagation of longitudinal-shear crack. *Zisin (J. Seismol. Soc. Jpn.)* 23: 304–12
Knopoff L. 1958. Energy release in earthquakes. *Geophys. J.* 1: 44–52
Kostrov BV. 1966. Unsteady propagation of longitudinal shear cracks. *Appl. Math. Mech.* 30: 1241–48
Kostrov BV. 1974. Seismic moment and energy of earthquakes, and seismic flow of rock. *Izv. Earth Phys.* 1: 23–40 (From Russian)
Lachenbruch AH, Sass JH.1973. Thermomechanical aspects of the San Andreas fault system. In *Proc. Conf. Tectonic Problems of the San Andreas Fault System*, ed. A. Nur, pp. 192–205. Stanford, CA: Stanford Univ. Press
Lachenbruch AH, Sass JH. 1980. Heat flow and energetics of the San Andreas fault zone. *J. Geophys. Res.* 85: 6185–222

Lay T, Kanamori H, Ruff L. 1982. The asperity model and the nature of large subduction zone earthquakes. *Earthquake Predict. Res.* 1: 3–71

Madariaga R. 1976. Dynamics of an expanding circular fault. *Bull. Seismol. Soc. Am.* 66: 639–66

Madariaga R. 1979. On the relation between seismic moment and stress drop in the presence of stress and strength heterogeneity. *J. Geophys. Res.* 84: 2243–50

McGuire RK, Hanks TC. 1980. RMS acceleration and spectral amplitudes of strong ground motion during the San Fernando, California earthquake. *Bull. Seismol. Soc. Am.* 70: 1907–19

Melosh J. 1979. Acoustic fluidization: a new geologic process? *J. Geophys. Res.* 84: 7513–20

Mendoza C, Hartzell SH. 1989. Slip distribution of the 19 September 1985 Michoacan, Mexico, earthquake: near-source and teleseismic constraints. *Bull. Seismol. Soc. Am.* 79: 655–69

Mikumo T, Hirahara K, Miyatake T. 1987. Dynamical fault rupture processes in heterogeneous media. *Tectonophysics* 144: 19–36

Miyamura S, Omote S, Teisseyre R, Vesanen E. 1964. Multiple shocks and earthquake series pattern. *Int. Inst. Seismol. Earthquake Eng. Bull.* 2: 71–92

Miyatake T. 1992a. Dynamic rupture process of inland earthquakes in Japan: weak and strong asperities. *Geophys. Res. Lett.* 19: 1041–44

Miyatake T. 1992b. Reconstruction of dynamic rupture process of an earthquake with constraints of kinematic parameters. *Geophys. Res. Lett.* 19: 349–52

Mogi K. 1968. Development of aftershock areas of great earthquakes. *Bull. Earthquake Res. Inst. Tokyo Univ.* 46: 175–203

Mount VS, Suppe J. 1987. State of stress near the San Andreas fault: implications for wrench tectonics. *Geology* 15: 1143–46

Munguia L, Brune JN. 1984. High stress drop events in the Victoria, Baja California earthquake swarm of 1978 March. *Geophys. J. R. Astron. Soc.* 76: 725–52

Orowan E. 1960. Mechanism of seismic faulting in rock deformation. *Geol. Soc. Am. Mem.* 79: 323–45

Quin H. 1990. Dynamic stress drop and rupture dynamics of the October 15, 1979 Imperial Valley, California, earthquake. *Tectonophysics* 175: 93–117

Rabinowicz E. 1965. *Friction and Wear of Materials*. New York: Wiley. 244 pp.

Rice JR. 1983. Constitutive relations for fault slip and earthquake instabilities. *Pageoph* 121: 443–75

Rice JR. 1991. Spatio-temporally complex fault slip: 3D simulations with rate- and state-dependent friction on a fault surface between elastically deformable continua. *Eos Trans. Am. Geophys. Union* 72: 278 (Abstr.)

Rice JR. 1992. Fault stress states, pore pressure distributions, and the weakness of the San Andreas fault. In *Fault Mechanics and Transport Properties of Rocks: A Festschrift in Honor of WF Brace*, ed. B Evans, W Teng-Fong, pp. 475–503. New York: Academic

Richards PG. 1976. Dynamic motions near an earthquake fault: a three-dimensional solution. *Bull. Seismol. Soc. Am.* 66: 1–32

Ruff L, Kanamori H. 1983. The rupture process and asperity distribution of three great earthquakes from long-period diffracted P-waves. *Phys. Earth Planet. Int.* 31: 202–30

Savage JC, Walsh JB. 1978. Gravitational energy and faulting. *Bull. Seismol. Soc. Am.* 68: 1613–22

Savage JC, Wood MD. 1971. The relation between apparent stress and stress drop. *Bull. Seismol. Soc. Am.* 61: 1381–88

Schallamach A. 1971. How does rubber slide? *Wear* 17: 301–12

Scholz CH. 1989. Mechanics of faulting. *Annu. Rev. Earth Planet. Sci.* 17: 309–34

Scholz CH. 1992. Paradigms or small change in earthquake mechanics. In *Fault Mechanics and Transport Properties of Rocks: A Festschrift in Honor of WF Brace*, ed. B Evans, W Teng-Fong, pp. 505–17. New York: Academic

Scholz CH, Aviles CA, Wesnousky SG. 1986. Scaling differences between large interplate and intraplate earthquakes. *Bull. Seismol. Soc. Am.* 76: 65–70

Schwartz S, Ruff L. 1987. Asperity distribution and earthquake occurrences in the southern Kurile Islands arc. *Phys. Earth Planet Int.* 49: 54–77

Sibson RH. 1973. Interactions between temperature and pore fluid pressure during faulting and a mechanism for partial or total stress relief. *Nature* 243: 66–68

Sibson RH. 1986. Rupture interaction with fault jogs. In *Earthquake Source Mechanics*, ed. S Das, J Boatright, CH Scholz, pp. 157–67. Washington, DC: Am. Geophys. Union

Sieh K, Jones L, Hauksson E, Hudnut K, Eberhart-Phillips D, et al. 1993. Near-field investigations of the Landers earthquake sequence, April to July 1992. *Science* 260: 171–76

Sieh KE. 1978. Slip along the San Andreas fault associated with the great 1857 earthquake. *Bull. Seismol. Soc. Am.* 68: 1421–57

Steidl JH, Archuleta RJ, Hartzell S. 1991. Rupture history of the 1989 Loma Prieta, California, earthquake. *Bull. Seismol. Soc. Am.* 81: 1573–602

Takeo M. 1988. Rupture process of the 1980 Izu-Hanto-Toho-Oki earthquake deduced from strong motion seismograms. *Bull. Seism. Soc. Am.* 78: 1074–91

Takeo M, Mikami N. 1987. Inversion of strong motion seismograms for the source process of the Naganoken-Seibu Earthquake of 1984. *Tectonophysics* 144: 271–85

Takeuchi H, Kikuchi M. 1971. On Kostrov's theory on crack propagation. *Geol. Eng.* 7: 13–19

Thatcher W. 1975. Strain accumulation and release mechanism of the 1906 San Francisco earthquake. *J. Geophys. Res.* 80: 4862–72

Thatcher W, Hanks TC. 1973. Source parameters of southern California earthquakes. *J. Geophys. Res.* 78: 8547–76

Tsuboi C. 1933. Investigation of deformation of the crust found by precise geodetic means. *Jpn. J. Astron. Geophys.* 10: 93–248

Udias A. 1991. Source mechainsm of earthquakes. *Adv. Geophys.* 33: 81–140

Vassiliou MS, Kanamori H. 1982. The energy release in earthquakes. *Seismol. Soc. Am. Bull.* 72: 371–87

Wald D. 1992. Strong motion and broadband teleseismic analysis of the 1991 Sierra Madre, California, earthquake. *J. Geophys. Res.* 97: 11,033–46

Wald DJ, Heaton TH. 1993. Spatial and temporal distribution of slip for the 1992 Landers, California, earthquake. *Bull. Seismol. Soc. Am.* Submitted

Wald DJ, Helmberger DV, Hartzell SH. 1990. Rupture process of the 1987 Superstition Hills earthquake from the inversion of strong-motion data. *Bull. Seismol. Soc. Am.* 80: 1079–98

Wald DJ, Helmberger DV, Heaton TH. 1991. Rupture model of the 1989 Loma Prieta earthquake from the inversion of strong-motion and broadband teleseismic data. *Bull. Seismol. Soc. Am.* 81: 1540–72

Wald DJ, Kanamori H, Helmberger DV, Heaton TH. 1993. Source study of the 1906 San Francisco earthquake. *Bull. Seismol. Soc. Am.* 83: 981–1019

Wyss M, Brune JN. 1967. The Alaska earthquake of 28 March 1964: a complex multiple rupture. *Bull. Seismol. Soc. Am.* 57: 1017–23

Wyss M, Molnar P. 1972. Efficiency, stress drop, apparent stress, effective stress, and frictional stress of Denver, Colorado, earthquakes. *J. Geophys. Res.* 77: 1433–38

Yamashita T. 1983. Peak and root-mean-square accelerations radiated from circular cracks and stress-drop associated with seismic high-frequency radiation. *J. Phys. Earth* 31: 225–49

Zoback MD, Zoback ML, Mount VS, Suppe J, Eaton J, et al. 1987. New evidence on the state of stress of the San Andreas fault system. *Science* 238: 1105–11

Annual Review of Earth and Planetary Sciences
Volume 22, 1994

CONTENTS